Aeroelastic Stability Analysis of Hingeless Rotor Blades with Composite Flexures

Sung Nam Jung
Department of Aerospace Engineering, Chonbuk National University, Chonju 561-756, Korea
Ki-Tae Kim, Seung Jo Kim*
School of Mechanical and Aerospace Engineering, Seoul National University, Seoul 151-742, Korea

The flap-lag-torsion coupled aeroelastic behavior of a hingeless rotor blade with composite flexures in hovering flight has been investigated by using the finite element method. The quasi-steady strip theory with dynamic inflow effects is used to obtain the aerodynamic loads acting on the blade. The governing differential equations of motion undergoing moderately large displacements and rotations are derived using the Hamilton's principle. The flexures used in the present model are composed of two composite plates which are rigidly attached together. The lead-lag flexure is located inboard of the flap flexure. A mixed warping model that combines the St. Venant torsion and the Vlasov torsion is developed to describe the twist behavior of the composite flexure. Numerical simulations are carried out to correlate the present results with experimental test data and also to identify the effects of structural couplings of the composite flexures on the aeroelastic stability of the blade. The prediction results agree well with other experimental data. The effects of elastic couplings such as pitch-flap, pitch-lag, and flap-lag couplings on the stability behavior of the composite blades are also investigated.

Key Words : Hingeless Rotor Blade, Composite Flexure, Hamilton's Principle, Aeroelastic Stability, Elastic Couplings

1. Introduction

Helicopters are susceptible to vibrations due largely to the rotational environment inherent in the vehicle for providing lift. Many studies have been focused to design more efficient and advanced geometry blades that lead to smaller parts, low weight, low drag, and also easy maintenance. One possible way to obtain this goal is the utilization of tailored composite flexures as a means to substitute the classical mechanical hinge structures, such as flap and lag hinges.

Bousman (1981, 1990) investigated experimentally the effects of a structural couplings on the stability of soft-inplane hingeless rotor. The experimental results were compared with a simplified rigid blade model. The pitch-lag and pitch-flap structural couplings were introduced by skewing the lag and flap flexures. The flap-lag coupling was obtained by inclining the flap and/or lag flexures at a specific angle with respect to the blade axis. The study showed that a combination of flap-lag and pitch-lag couplings was beneficial to blade stability. It is noted that the flexure materials used in the study are confined to isotropic materials and the theoretical results used in the comparison are only for a rigid blade.

A series of analyses have been conducted to consider the effects of elastic couplings on the

* Corresponding Author,
E-mail : sjkim@snu.ac.kr
TEL : +82-2-880-7388; **FAX** : +82-2-880-2662
School of Mechanical and Aerospace Engineering, Seoul National University, Seoul 151-742, Korea.
(Manuscript **Received** August 10, 2001; **Revised** January 7, 2002)

stability behavior of composite rotors. Hong and Chopra (1985) used a simple kinematic model of a composite blade to examine the effects of elastic couplings on the aeroelastic stability in hover. Smith and Chopra (1993) extended this work to include the nonclassical structural effects such as transverse shear, torsion warping, and two-dimensional inplane elasticity. Jung and Kim (1996) introduced the shear correction factor to account for the sectional distribution of shear and improved the prediction of transverse shear behavior of a composite rotor. Tracy and Chopra (1995) and Floros and Smith (1996) have focused on the development of torsion related warping restraint model for the analysis of open-section composite beams.

Tracy and Chopra (1996) investigated the aeroelastic stability behavior of composite hingeless rotors by using a composite flexure. The fundamental idea of using the composite flexure in this study was to replace the mechanical flap and lag hinges in the blade system. They used an effective modulus approach in predicting structural properties of the flexure and combined the results with UMARC (University of Maryland Advanced Rotorcraft Code) to perform the aeroelastic analysis (Bir and Chopra, 1994). In the effective modulus approach, an experimental test must be performed a priori to obtain the stiffness properties of the composite flexures. Generally, the procedures to obtain the stiffness properties by experimental tests need much effort and take more time in comparison with an analytical method. But, in the analysis method, the non-classical structural effects such as transverse shear and constrained warping appear to be very important and must be incorporated appropriately in the analysis, because of the fact that the flexures are subjected to large periodic motions, heavy inertial loads, and cyclic torsional moments.

In the present work, the aeroelastic behavior of a hingeless rotor blade with composite flexures is studied. Special care is taken to improve the helicopter rotor performance through the appropriate design of flexures. The flexures used in the present model are composed of two composite plates which are rigidly attached together. The flexure configuration is adopted from the work of Bousman (1990). A mixed warping model that combines the St. Venant torsion with Vlasov torsion is developed to describe the torsion response of the composite flexure. The damped element model of Lin et al. (1984) is also incorporated to determine the structural damping parameters such as modal damping ratios. The objectives of the current work are: 1) to construct a consistent analysis method to capture the nonclassical behavior of composite flexures; and 2) to investigate the elastic coupling behavior of composite flexures on the aeroelastic stability.

2. Formulation

2.1 Composition of motion equations

Consider a hingeless helicopter blade rotating with constant angular velocity Ω, as depicted in Fig. 1. Two Cartesian coordinate systems are used to describe the motion of the blade: the x-y-z undeformed coordinate system and the $\xi-\eta-\zeta$ deformed coordinate system. The deformation of the blade in space is described by the displacements u, v, w, and ϕ that are axial, lead-lag, flap, and elastic twist deformations, respectively.

The strain-displacement relations for small strains and moderately large deformations, up to second order, can be obtained in terms of displacement derivatives in the following form

$$\varepsilon_{xx}=u'+\frac{v'^2}{2}+\frac{w'^2}{2}-\lambda_T\phi''+(\eta^2+\zeta^2)\left(\theta'_0\phi'+\frac{\phi'^2}{2}\right)$$

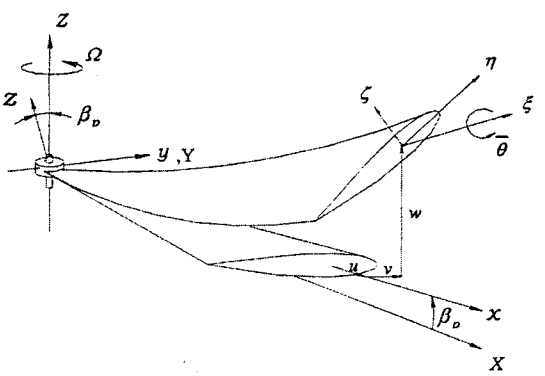

Fig. 1 Rotor blade geometry and deformations

$$-v^n(\eta\cos\bar{\theta}-\zeta\sin\bar{\theta})$$
$$-w^n(\eta\sin\bar{\theta}+\zeta\cos\bar{\theta}) \quad (1)$$
$$\varepsilon_{x\eta}=-\left(\zeta+\frac{\partial\lambda_T}{\partial\eta}\right)\phi'$$
$$\varepsilon_{x\zeta}=\left(\eta-\frac{\partial\lambda_T}{\partial\zeta}\right)\phi'$$

where $\bar{\theta}$ is the total geometric pitch of the blade, θ_0 is the twist angle, and λ_T is the torsion-related warping function.

Figure 2 shows the schematic of a hingeless rotor blade with flap and lead-lag flexures. The flexures used in the present model are composed of two composite plates which are rigidly attached together. The lead-lag flexure is located inboard of the flap flexure. The current flexure model is similar to the flexure configuration used in the experimental study conducted by Bousman (1990). Structural couplings such as pitch-flap and pitch-lag couplings are introduced herein by changing the fiber orientation angles in the composite flexures. While in the work of Bousman, the flexures were made of isotropic materials and the structural couplings were obtained by skewing the flexures in a purely geometric manner. But, in both studies, the flap-lag type of couplings could be achieved by inclining the flexures relative to the main blade.

The constitutive relations for the flap and the lead-lag flexures are respectively of the following form

$$\begin{Bmatrix}\sigma_{xx}\\ \sigma_{x\eta}\end{Bmatrix}=\begin{bmatrix}C_{11} & C_{16}\\ C_{16} & C_{66}\end{bmatrix}\begin{Bmatrix}\varepsilon_{xx}\\ \varepsilon_{x\eta}\end{Bmatrix} \quad (2a)$$
$$\sigma_{xs}=C_{55}\varepsilon_{xs}$$

for the flap flexure and

$$\begin{Bmatrix}\sigma_{xx}\\ \sigma_{x\zeta}\end{Bmatrix}=\begin{bmatrix}C_{11} & C_{16}\\ C_{16} & C_{66}\end{bmatrix}\begin{Bmatrix}\varepsilon_{xx}\\ \varepsilon_{x\zeta}\end{Bmatrix} \quad (2b)$$
$$\sigma_{x\eta}=C_{55}\varepsilon_{x\eta}$$

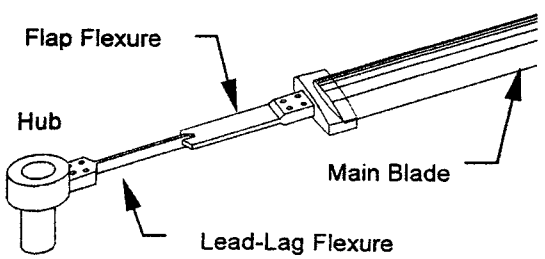

Fig. 2 Schematic of the hingeless rotor with flexures

for the lag flexure. In the above Eq. (2), the stiffness coefficients C_{ij} are defined as

$$C_{ij}=\bar{Q}_{ij}-\frac{\bar{Q}_{i2}\bar{Q}_{2j}}{\bar{Q}_{22}} \text{ for } i,\ j=1,\ 6 \quad (2c)$$
$$C_{55}=\bar{Q}_{55}$$

where the expression for the transformed reduced stiffness matrix $\bar{Q}_{ij}$ in terms of material constants can be found in Jones (1975).

The governing differential equations of motion for the composite hingeless blade can be derived by using the Hamilton's energy principle

$$\int_{t_1}^{t_2}(\delta U-\delta T-\delta W_e)\,dt=0 \quad (3)$$

where δU, δT, and δW_2 are the strain energy variation, the kinetic energy variation, and the external virtual work, respectively, and they are defined as

$$\delta U=\int_0^R\iint_A(\sigma_{xx}\delta\varepsilon_{xx}+\sigma_{x\eta}\delta\varepsilon_{x\eta}+\sigma_{x\zeta}\delta\varepsilon_{x\zeta})\,dA\,dx \quad (3a)$$

$$\delta T=\int_0^R\iint_A\rho V\cdot\delta V\,dA\,dx \quad (3b)$$

$$\delta W_e=\int_0^R(L_u\delta u+L_v\delta v+L_w\delta w+M_\phi\delta\phi)\,dx \quad (3c)$$

where A is the cross-section area of the blade and R is the blade length. In the kinetic energy expression, V is the velocity vector for a given point on the deformed frame and ρ is the mass density of the blade. On the right-hand side of Eq. (3c), L_u, L_v, L_w, and M_ϕ are the aerodynamic components in the respective motion of the blade.

2.2 Warping function

The warping deformation of a beam section is composed of the warping of the contour and the warping of the wall relative to the contour (Gjelsvik, 1981). The latter is called the thickness warping. Depending on the stiffness properties and the geometry of the beam section, a different combination of warping deformations needs to be taken into account. The present flexure model has a narrow rectangular section. Also, due to double

symmetry nature of the section, the principal pole and the origin coincide with the area center. Therefore the total warping for the rectangular solid section leads to thickness warping only. The warping function for the section is expressed in the form of (Ritchie and Rosinger, 1975)

$$\lambda_T=\eta\varsigma-\tanh\left(\frac{\pi}{2}\cdot\frac{b}{t}\cdot\sqrt{\frac{G_{xy}}{G_{xz}}}\right)\Big/\left(\frac{2}{\pi}\cdot\frac{t}{b}\cdot\sqrt{\frac{G_{xz}}{G_{xy}}}\right) \quad (4)$$

where G_{xz}/G_{xy} is the ratio of shear moduli referred to as the blade axes. On the right-hand side of Eq. (4), the first term represents the linear warping and the second term represents the higer order contribution of the thickness warping. This equation is a purely unrestrained torsion solution (i.e., St. Venant solution.) In case the beam is relatively short and is constrained at either end or both ends of the beam, local restraint effects can be significant and should be considered appropriately. In order to deal with this specific case, more general treatment of torsion problem is needed and the details are presented in this section.

The governing differential equation of a general torsion problem is given by the relation

$$EI_{\Omega\Omega}\phi'''-GJ\phi'=-T \quad (5)$$

where $EI_{\Omega\Omega}$ is the Vlasov warping constant, GJ is the torsional rigidity, and T is the torque load applied at the beam tip. The torque component consists of two parts: Vlasov torsion T_Ω and St. Venant torsion T_S an. The relative values of T_S and T_Ω are defined as (Gjelsvik, 1981)

$$\left|\frac{T_S}{T_\Omega}\right|=\mu^2\frac{d\phi/d\bar{x}}{d^3\phi/d\bar{x}^3} \quad (6)$$

where

$$\bar{x}=\frac{x}{l_f} \quad (6a)$$

$$\mu=\frac{l_f}{\delta} \quad (6b)$$

$$\delta=\sqrt{\frac{EI_{\Omega\Omega}}{GJ}} \quad (6c)$$

where l_f is the length of the flexure. The parameter δ has a unit of length and is called the characteristic length of a beam. The nondimensional beam parameter μ appeared in Eq. (6c) is crucial in describing the magnitude of warping and depends on the geometry, boundary conditions, and stiffness properties of the beam. For composite beams with rectangular cross-section having width b and thickness t, the Vlasov warping stiffness and the torsional rigidity are obtained respectively as (Bauld and Tzeng, 1984)

$$EI_{\Omega\Omega}=\int_{-t/2}^{t/2}\int_{-b/2}^{b/2}C_{11}\eta^2\varsigma^2 d\eta d\varsigma$$
$$GJ=\int_{-t/2}^{t/2}\int_{-b/2}^{b/2}4C_{66}\varsigma^2 d\eta d\varsigma \quad (7)$$

where C_{11} and C_{66} are defined in Eq. (2c). The flexure model is cantilevered at its root and warping restrained at both ends of the beam, as depicted in Fig. 2. This boundary condition is applicable to the present flexure models, where the root is attached to the rotor hub and the other end is connected to the main rotor blade. Considering this boundary condition into the mixed torsion equation, one can get the twist solution as

$$\phi=f_M T \quad (8)$$

where the mixed torsion flexibility, f_M, is denoted by using the St. Venant torsion flexibility $f_S(=l_f/GJ)$ as

$$f_M=\frac{1}{\mu}\left[\frac{(\cosh\mu-1)^2}{\sinh\mu}-\sinh\mu+\mu\right]f_S \quad (9)$$

The ratio of the mixed torsion flexibility to the St. Venant one is presented in Fig. 3 as a

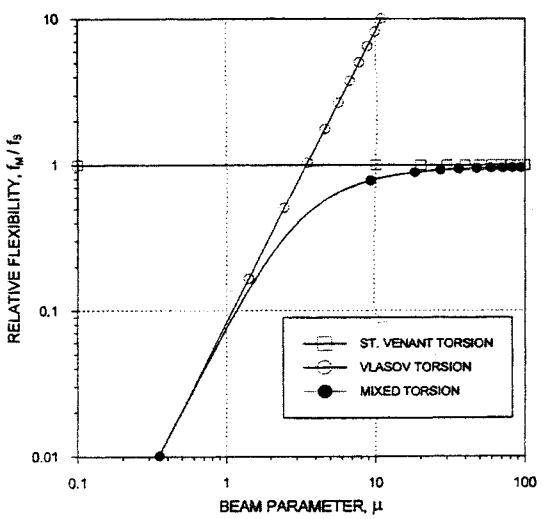

Fig. 3 Relative torsional flexibility of beams

function of the beam parameter μ. When μ is near unity, pure Vlasov torsion is a good approximation to the torsion solution. When μ is large compared to unity, St. Venant torsion is a good approximation to the torsion solution. But in the moderate values of μ, the mixed torsion solution is needed. Considering the boundary conditions with one end fixed and both ends warping restrained, the twist solution for the beam under the tip torque is obtained as

$$\phi=\frac{T\cdot\delta}{GJ}\left[\frac{x}{\delta}-\sinh\left(\frac{x}{\delta}\right)+\frac{(\cosh\mu-1)}{\sinh\mu}\left\{\cosh\left(\frac{x}{\delta}\right)-1\right\}\right] \tag{10}$$

where the first term in the brackets represents the St. Venant solution and the second and third terms in the brackets represent the Vlasov torsion solution.

2.3 Finite element solution

The blade structure is discretized into a number of beam finite elements. Each beam finite element is composed of 15 degrees of freedom to fully consider the extension-flap-lag-torsion coupled behavior of the blade. Applying the finite element method to the Hamilton's principle (Eq. (3)), one obtains the nonlinear finite element equations of motion in terms of nodal degrees of freedom $\boldsymbol{q}$ as

$$\boldsymbol{M}\ddot{\boldsymbol{q}}+\boldsymbol{C}(\boldsymbol{q})\dot{\boldsymbol{q}}+\boldsymbol{K}(\boldsymbol{q})\boldsymbol{q}=\boldsymbol{F} \tag{11}$$

where $\boldsymbol{M}$, $\boldsymbol{C}$, $\boldsymbol{K}$, and $\boldsymbol{F}$ are the global inertia, damping, stiffness matrices and load vector, respectively. The transverse shear flexibility is omitted in the finite element equations for simplicity. The nonlinear equations of motion, Eq. (11), are solved iteratively by using the Newton-Raphson technique. Next, a modal coordinate transformation based on the normal modes, which are determined from rotating free vibration analysis, is applied as a means of saving computation time in the subsequent stability analysis. In order to consider the low-frequency unsteady aerodynamic effects in the stability analysis, a dynamic inflow model by Pitt and Peters (1981) is used. Finally, the stability analysis of the blade is conducted from the modal flutter equations, which are transformed to a first-order system and solved as an algebraic eigenvalue problem (Jung and Kim, 1996).

3. Results and Discussion

3.1 Composite flexure

The present beam finite element solutions for the composite flexure under a tip bending load are correlated against the detailed finite element results using the ABAQUS. The comparison is conducted for beams with bending-torsion couplings. The geometry and the lamination configurations for the composite flexure are depicted in Fig. 4. The flexure model is 1.2 inches long and 0.5 inches wide. The model is loaded with a tip bending load of 10 *in-lb* and is cantilevered at its root and warping restrained at both ends. Figure 5 shows the shell finite element meshes used in the ABAQUS calculation. In order to simulate the warping restrained condition in the ABAQUS

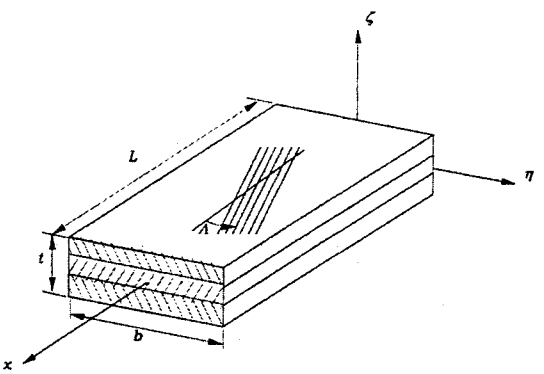

Fig. 4 Geometry of the composite flexure

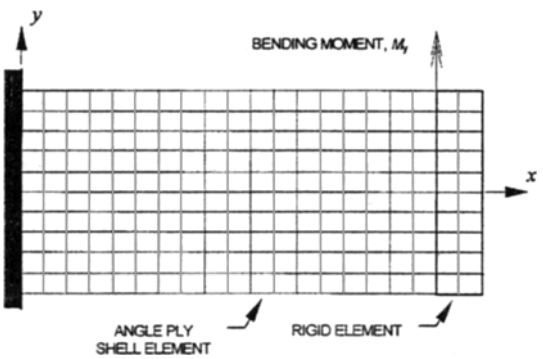

Fig. 5 Two-dimensional shell finite element meshes for the ABAQUS

Table 1 Mechanical properties of graphite-epoxy lamina

Property	Value
E_1, msi	18.85
E_2, msi	1.392
G_{12}, G_{13}, msi	0.696
G_{23}, msi	0.464
ν_{12}	0.31
ρ, lb/in^3	0.05672
Ply thickness, t, in	0.005

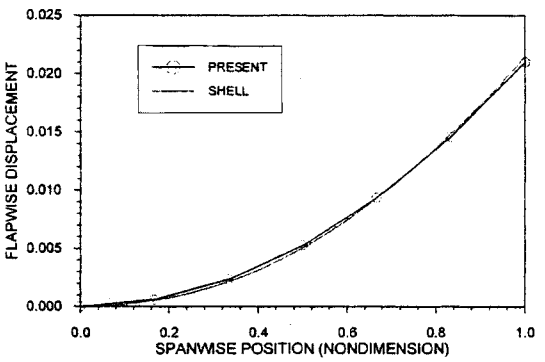

Fig. 6 Comparison of flapwise displacements under 10 in-lb tip bending load

analysis, a series of rigid elements are attached near the beam tip, as seen in Fig. 5. Figure 6 shows the comparison results between the current predictions and the shell finite element solutions obtained each for flapwise displacements. The ply lay-up for the composite beam is set to $[15_5^\circ/0_7^\circ/15_5^\circ]$. The positive fiber angle is defined as the right angle about the ζ-axis of the beam. The materials used are CU-125 graphite-epoxy and their mechanical properties are presented in Table 1. The detailed finite element model was composed of 200 quadrilateral shell elements including 20 rigid elements, while the present beam model used six beam finite elements. It is seen in Fig. 6 that the present beam analysis results are in a good agreement with those of the detailed finite element analysis.

Figure 7 shows the bending-torsion coupled response of the beam, which is subjected to 10 *in-lb* tip bending load. The lay-up angle for this case is $[\Lambda_5/0_7^\circ/\Lambda_5]$, where Λ is varied from 0° to 90°. Fairly good correlation is obtained between

Table 2 Rotor blade properties

Number of blades	2
Rotor radius, R, in	31.92
Blade chord, c, in	1.65
Blade airfoil	NACA 23012
Hinge offset, e	0.105
Solidity ratio, σ	0.033
Lock number, γ	7.99
Rotor speed, Ω, RPM	682

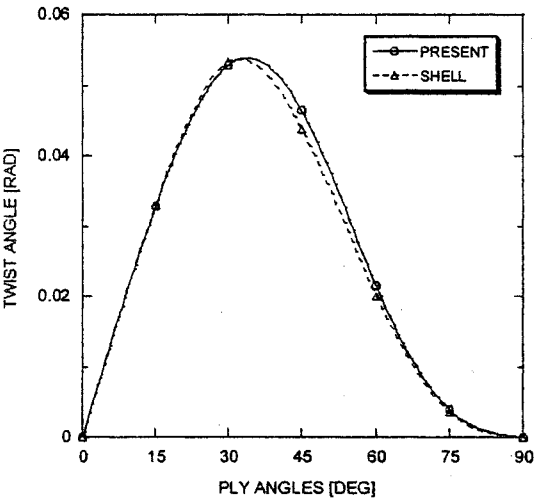

Fig. 7 Comparison of twist deformations under 10 in-lb tip bending load

the two finite element results. The maximum error is 7% at the fiber angle of 45°. The above analysis results indicate that the present composite beam model is accurate enough for use in the comprehensive aeroelastic analysis of hingeless helicopter blades.

3.2 Isotropic hingeless rotor blade

A Froude-scaled, two-bladed hingeless blade with a straight flap and lead-lag flexures is investigated in this section. The model was used in an experimental study conducted by Bousman (1994). The flexures of the model were made of isotropic materials and their respective centerlines were designed to be coincident with each other. The model rotor had stiffness in torsion to decouple the torsion mode from other flap and lead-lag modes. The rotor configuration and the experimental details can be found in Bousman

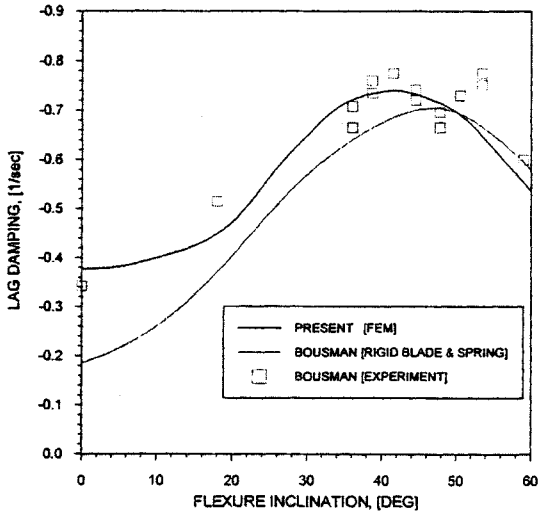

Fig. 8 Lag mode damping for hingeless blades with metal flexures as a function of flexure inclination angles

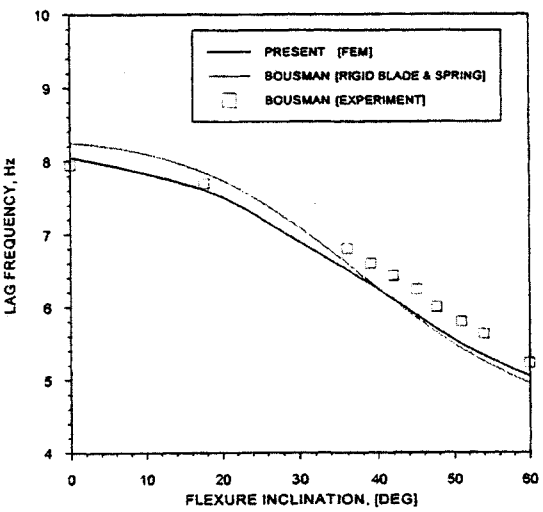

Fig. 9 Lag mode frequency for hingeless blades with metal flexures as a function of flexure inclination angles

(1990). The rotor properties used in the calculation are summarized in Table 2.

Figure 8 shows the comparison results for the aeroelastic stability of the model blade with metal flexures. In order to identify the stability behavior of a blade, the lag mode damping is plotted against the flexure inclination angles. The test data appeared in the comparison were obtained from Bousman (1990). The current finite element results are denoted in solid lines, while the experimental results and the rigid blade analysis results of Bousman are expressed in rectangles and dotted lines, respectively. For the present results, ten spanwise beam finite elements including two finite elements for each of the flexures are used. Five normal modes (three flap and two lag modes) are used for stability analysis. The stiffness properties for the lead-lag and flap flexures were determined from the equivalence of the bending slope and twist angles between the experimental model and the current elastic beam model. The section properties of the main blade and the flexures used in the calculation are given in Table 3. These structural properties represent a soft-inplane, Froude-scaled hingeless blade with ν_S=0.7/rev. As seen from Fig. 8, the effect of flexure inclination is to increase the lead-lag damping until a maximum value is reached, which occurs at around 45 degrees. Good correlation for the lead-lag damping responses between the current predictions and the experimental results is clearly seen in the plot.

Figure 9 presents the variation of lead-lag frequencies with respect to the flexure inclination angles. Good correlation with experiments is also apparent through the use of the current beam finite element approach.

3.3 Composite hingeless rotor blade

Figure 10 shows the stability results of a composite hingeless blade with changing fiber orientation angles. The lay-up angles for the lead-lag and the flap flexures are and $[\Lambda_3/(15°/-15°)/0_3^\circ]_S$ and $[90_3^\circ/(15°/-15°)_3/0_2^\circ]_S$, respectively, which represent the chordwise bending-torsion coupling. The lamination configuration for the flexure was determined to represent realistic blade properties. The baseline rotor has a soft-inplane characteristic with a stiff torsion like the Bousman model (Bousman, 1990). The rotating natural frequencies for the baseline blade are respectively obtained as: ν_β=1.14/rev, ν_ζ=0.66/rev, and ν_ϕ= 10.2/rev. The blade structure is composed of zero ply angles to prevent the elastic motions of the blade from mixing with those of the composite flexures. The stiffness properties of the blade used

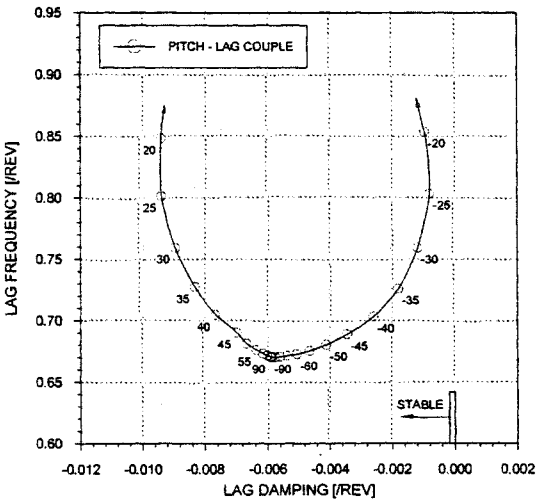

Fig. 10 Root locus plots for the pitch-lag coupled configuration

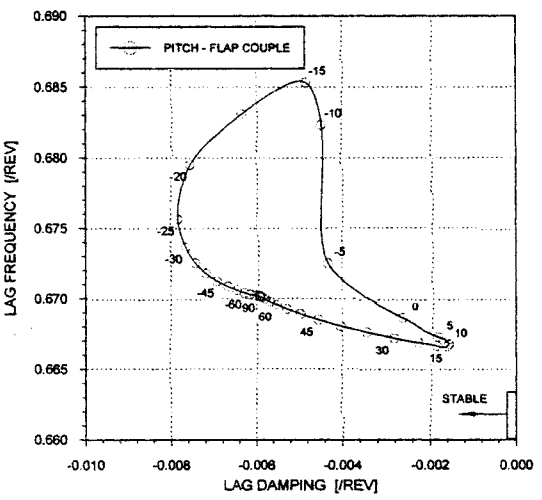

Fig. 11 Root locus plots for the pitch-flap coupled configuration

in the calculation are given in Table 3. Six normal modes (3 flap, 2 lag, and 1 torsion) were used to perform stability analysis. It is seen in Fig. 10 that the fiber orientation angles of the composite flexure have substantial effects on both the lag mode frequency and damping. The positive fiber angles representing the negative pitch-lag coupling (lag back-pitch up) show significant stabilizing effects, while the negative fiber angles destabilize the motion. The stability results for fiber angles below 20 degrees in absolute values are not presented in the plot because the frequency values become unrealistic for those angles.

In Fig. 11, the root loci of complex eigenvalues are plotted against the fiber orientation angles for the case of pitch-flap coupling. In this case, the lay-up angles of the flap flexure are set to $[\Lambda_3/(15°/-15°)_3/0_3^\circ]$, while the lag flexure has a layup of $[90_3^\circ/(15°/-15°)_3/0_2^\circ]_s$. This configuration represents the flapwise bending-torsion coupling. The effect of ply angle changes of the flap flexures on the lag mode damping is observed to be substantial as seen in the plot. The positive ply angles representing the positive pitch-flap coupling (flap up-pitch down) destabilize the lag mode substantially as the ply angle changes. A marginal damping value is obtained near the fiber angle of 10 degrees. On the other hand, the negative ply angles stabilize the lag mode in some

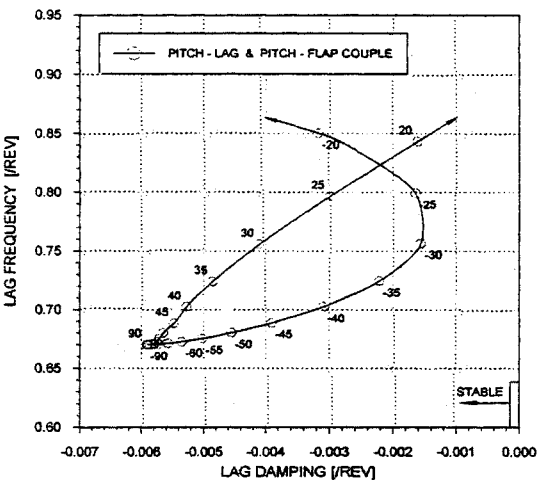

Fig. 12 Root locus plots for both the pitch-lag and pitch-flap coupled configurations

degree with the introduction of the negative pitch-flap coupling.

Figure 12 shows the stability results of combined pitch-flap and pitch-lag coupled blades. In this case, the ply lay-up for the flap flexure is set to $[\Lambda_3/(15°/-15°)_3/0_3^\circ]_s$, while the lag flexure has a layup of $[\Lambda_3/(15°/-15°)_3/0_2^\circ]_s$. For this configuration, the ply angles for both the flexures vary at once. The effect of ply angle changes for the flexures on the lag mode damping appears quite large. Mixed results of both the pitch-flap and pitch-lag couplings are observed in the plot.

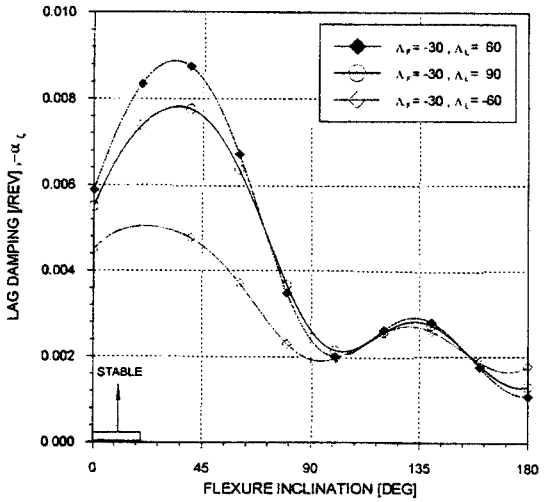

Fig. 13 Lag mode damping for composite blades with pitch-flap and pitch-lag couplings as a function of flexure inclination angles

Numerical results of the geometric flap-lag coupling along with the pitch-flap and pitch-lag couplings are illustrated in Fig. 13, where the lead-lag damping values are presented as a function of flexure inclination angles for three different flexure configurations. In all three cases, the lay-up geometry for the flap flexure is set to $[-30^\circ_3/(15^\circ/-15^\circ)_3/0^\circ_3]_S$, which results in maximum damping for the pitch-flap coupling alone, whereas the lay-up angles of the lead-lag flexure vary with -60, 90 and 60 degrees. A harmonic variation of damping is noticed with the introduction of the flap-lag coupling. As the flexure inclination angle reaches above 90 degrees, the variation of lead-lag damping becomes smaller than that with the low flexure inclination angles. At these flexure inclination angles, the effects of flap-lag coupling on the lag mode damping seem to be canceled with the elastic bending-torsion coupling. Among the three flexure configurations, the case with a ply angle of 60 degrees in the lag flexure is seen to have maximum damping at a flexure inclination of 30 degrees.

4. Concluding Remarks

In the present work, the hover aeroelastic stability of a hingeless rotor blade with composite flexures has been investigated by using the finite element method. The quasi-steady strip theory with dynamic inflow effects was used to obtain the aerodynamic loads acting on the blade. The governing differential equations of motion undergoing moderately large displacements and rotations were derived using the Hamilton's principle. A mixed warping model that combines the St. Venant torsion with Vlasov torsion was developed to describe the twist behavior of the composite flexure. Based on the current work, the following conclusions are drawn:

(1) The present beam model that takes into account the warping restraint effect through mixed torsion theory has been correlated successfully with detailed shell finite element solutions. In addition, the aeroelastic stability results for a Froude-scaled hingeless blade with metal flexures are correlated well with experimental test data.

(2) The negative pitch-lag coupling (lag back-pitch up) has a strong stabilizing effect on the lag mode damping and the negative pitch-flap coupling (flap up-pitch up) stabilizes the lag motion substantially. The elastic couplings can play a significant role on stability behavior of the lag mode.

(3) The combined effects of geometric plus elastic couplings, which are induced respectively by flexure inclinations and non-zero ply angles of the blade, appear quite significant on the aeroelastic stability results and systematic study is needed to obtain the best combination of the structural couplings.

Acknowledgment

This study has been supported by National Research Laboratory Programs under the contract No. 00-N-NL-01-C-026.

References

Bauld, N. R., Jr. and Tzeng, L. S., 1984, "A Vlasov Theory for Fiber-Reinforced Beams with Thin-Walled Open Cross Sections," *International Journal of Solids and Structures*, Vol. 20, No. 3,

pp. 277~297.

Bir, G. and Chopra, I., 1994, *University of Maryland Advanced Rotorcraft Code (UMARC)*, Center for Rotorcraft Education and Research, University of Maryland, College Park.

Bousman, W. G., 1981, "An Experimental Investigation of the Effects of Aeroelastic Couplings on Aeromechanical Stability of a Hingeless Rotor Helicopter," *Journal of the American Helicopter Society*, Vol. 26, No. 1, pp. 46~54.

Bousman, W. G., 1990, "The Effects of Structural Flap-Lag and Pitch-Lag Coupling on Soft Inplane Hingeless Rotor Stability in Hover" NASA TP 3002, AVSCOM TR 89-A-002.

Floros, M. W. and Smith, E. C., 1996, "Finite Element Modeling of Open-Section Composite Beams with Warping Restraint Effects," *Proceeding of 37th Structures, Structural Dynamics, and Materials Conferences*, Salt Lake City, pp. 1420~1430.

Gjelsvik, A., 1981, *The Theory of Thin Walled Bars*, John Wiley & Sons.

Hong, C. H. and Chopra, I., 1985, "Aeroelastic Stability Analysis of a Composite Rotor Blade," *Journal of the American Helicopter Society*, Vol. 30, No. 2, pp. 57~67.

Jones, R. M., 1975, *Mechanics of Composite Materials*, McGraw-Hill, New York.

Jung, S. N. and Kim, S. J., 1996, "Transverse Shear Behavior on the Aeroelastic Stability of Composite Rotor Blade," *KSME International Journal*, Vol. 10, No. 1, pp. 12~21.

Lin, D. X., Ni, R. G. and Adams, R. D., 1984, "Prediction and Measurement of the Vibrational Damping Parameters of Carbon and Glass-Fiber Reinforced Plastics Plates," *Journal of Composite Materials*, Vol. 18, pp. 132~152.

Pitt, D. M. and Peters, D. A., 1981, "Theoretical Prediction of Dynamic Inflow Derivatives," *Vertica*, Vol. 5, No. 1, pp. 21~34.

Ritchie, I. G. and Rosinger, H. E., 1975, "Torsional Rigidity of Rectangular Section Bars of Orthotropic Materials," *Journal of Composite Materials*, Vol. 9, pp. 187~190.

Smith, E. C. and Chopra, I., 1993, "Aeroelastic Response, Loads and Stability of a Composite Rotor in Forward Flight," *AIAA Journal*, Vol. 31, No. 7, pp. 1265~1273.

Tracy, A. L. and Chopra, I., 1995, "Aeroelastic Analysis of a Composite Bearingless Rotor in Forward Flight Using an Improved Warping Model," *Journal of the American Helicopter Society*, Vol. 40, No. 3, pp. 80~91.

Tracy, A. L. and Chopra, I., 1996, "Aeroelastic Stability Testing and Validation of a Composite Hingeless Rotor in Hover," *Proceeding of 37th Structures, Structural Dynamics, and Materials Conferences*, Salt Lake City, pp. 2447~2458.